Quantum-size confinement of excitons in CuBr nanocrystals embedded in a polymer

2001 J. Phys.: Condens. Matter 13 11465

(http://iopscience.iop.org/0953-8984/13/50/306)

INSTITUTE OF PHYSICS PUBLISHING JOURNAL OF PHYSICS: CONDENSED MATTER

J. Phys.: Condens. Matter **13** (2001) 11465–11472 PII: S0953-8984(01)28224-1

Quantum-size confinement of excitons in CuBr nanocrystals embedded in a polymer

M Oda, M Y Shen, M Saito and T Goto

Department of Physics, Graduate School of Science, Tohoku University, Sendai 980-8578, Japan

Received 22 August 2001, in final form 11 October 2001
Published 30 November 2001
Online at stacks.iop.org/JPhysCM/13/11465

Abstract

Quantum-size confinement of excitons in CuBr nanocrystals embedded in polymethyl methacrylate has been studied. Both the absorption band and the photoluminescence (PL) band of the $Z_{1,2}$ free excitons in the nanocrystals show a blue-shift due to a quantum-size effect, and the Stokes shift of the PL band becomes larger with decrease in the nanocrystal size at 77 K. These blue-shifts are interpreted by application of size quantization in the exciton dispersion on the basis of Cho's $\boldsymbol{k}$-linear theory.

1. Introduction

Cuprous halide nanocrystal is one of the most widely used materials for study of quantum-size confinement of exciton translational motion.

The exciton absorption spectra of bulk crystals of the cuprous halides CuCl, CuBr, and CuI consist of two intense narrow bands, which are called $Z_{1,2}$ and Z_3 bands [1]. The energy of the Z_3 exciton band is lower than that of the $Z_{1,2}$ exciton in CuCl, while the energy of the $Z_{1,2}$ exciton is lower than that of the Z_3 exciton in CuBr and CuI, because the contribution of the copper ion with negative spin–orbit interaction to the valence band is larger in CuCl than in CuBr and CuI. The $Z_{1,2}$ exciton in CuBr with a zinc-blende structure is associated with Γ_8 hole and Γ_6 electron states, and is composed of Γ_5 and $\Gamma_3 + \Gamma_4$ states [1, 2]. The Γ_5 state with threefold degeneracy is a dipole-allowed spin-singlet state and splits into a longitudinal exciton state and a transverse exciton state with twofold degeneracy by a dipole–dipole interaction. The $\Gamma_3 + \Gamma_4$ state with fivefold degeneracy is a dipole-forbidden spin-triplet state. The $\Gamma_3 + \Gamma_4$ exciton, however, becomes partially allowed because of the exchange interaction and the $\boldsymbol{k}$-linear term, where $\boldsymbol{k}$ is the wave vector of the exciton translational motion. A sharp peak observed on the low-energy side of the $Z_{1,2}$ reflection structure at 8 K is assigned to the $\Gamma_3 + \Gamma_4$ exciton [3]. Below 50 K, the photoluminescence (PL) band associated with this state is easily observed because this state has the lowest energy.

0953-8984/01/5011465+08$30.00

In CuCl nanocrystals, the size dependence of the Z_3 exciton energy can be explained by an exciton confinement model described as

$$\Delta E = \frac{\hbar^2}{2m}\left(\frac{\pi}{R-d}\right)^2 \tag{1.1}$$

where ΔE is a blue-shift of the exciton energy, m is the exciton translational mass [4], R is the radius of the nanocrystal, and d is a depth of the dead layer into which the centre of mass of an exciton cannot enter.

In CuBr nanocrystals, the $Z_{1,2}$ exciton level splits into multiple levels and the exciton energies shift to the higher-energy side due to a quantum-size effect [5]. The size dependence of the blue-shift in CuBr nanocrystals, however, has not been fitted by equation (1.1). It is not clear why the size dependence in CuBr nanocrystals is not explained by this simple model at present.

At 77 K, the Stokes shift of the PL due to the Z_3 exciton in the CuCl nanocrystal equals zero [6], because the exciton bound to an impurity or a defect is unstable at this temperature and the Γ_5 free exciton annihilates radiatively. In contrast, in the CuBr nanocrystal, a finite Stokes shift appears even at 77 K [7], but the origin is not clear at present.

The key to clarifying the quantum-size effects in CuBr nanocrystals lies in the multiplicity of the $Z_{1,2}$ exciton. Itoh *et al* reported on size-quantized excitons in microcrystals of cuprous halides embedded in alkali halide matrices [8]. In their paper, excitation spectra of broad $Z_{1,2}$ exciton luminescence bands are measured, and it is suggested that the $Z_{1,2}$ exciton is mainly composed of three exciton states in thin platelet microcrystals which have $\langle 111 \rangle$ flat surfaces. The existence of the three exciton states is explained by a rough calculation taking the $\boldsymbol{k}$-linear term into account.

In this paper, the size dependence of the absorption band energy and the PL band energy of the $Z_{1,2}$ exciton in the CuBr nanocrystal are discussed more strictly on the basis of size quantization of the exciton translational motion in the exciton dispersion calculated in terms of a $\boldsymbol{k}$-linear theory.

2. Experiment

In the present experiment, we used CuBr nanocrystals embedded in polymethyl methacrylate (PMMA). The samples were prepared by Yao's technique [9]. The size of the nanocrystallites was controlled by heat treatment. The weight concentration of the nanocrystal in the PMMA film was about 0.18% and the film thickness was typically about 0.4 mm. In order to obtain the transmission electron microscope (TEM) images of the nanocrystals, the samples were sliced to a thickness of about 60 nm and the samples were then coated with carbon to prevent the film from being charged by the electron beam. We determined the sizes and shapes of CuBr nanocrystals embedded in ten films in pictures taken with a Hitachi H-9000NAR TEM. For optical measurements, the PMMA film was immersed in liquid nitrogen. For PL measurements, the samples were excited by a 325 nm cw light from a He–Cd laser with an intensity of 10 mW cm^{-2} on the sample surface. The absorption and photoluminescence spectra were measured with an Acton Spectra Pro-500 single monochromator and a Hamamatsu C4196 silicon photodiode array. The spectral resolution of the measurement system was 3 meV.

3. Results and discussion

Figure 1 shows a TEM picture of a sample. As can be seen in the picture, the nanocrystal is approximately spherical in shape. The average radius ($\bar{R}$) of the CuBr nanocrystals in this

figure is 7.0 ± 1.5 nm, and a histogram of the sample size is shown in figure 2. The optical absorption spectra at 77K of ten samples, which were taken using the TEM, are shown in figure 3. The volume average radius ($\bar{R}_v$) of each nanocrystal is shown on the left-hand side of each spectrum. Considering that the exciton absorption strength (band area) and the PL intensity are proportional to the volume of a nanocrystal, the volume average radius of each sample should be used as the average radius in the discussion below. The lower- and higher-energy bands are associated with the $Z_{1,2}$ and Z_3 excitons, respectively. The broadness of the band is mainly due to inhomogeneity of the nanocrystal size. Both of the exciton bands shift to the higher-energy side when the nanocrystal size decreases. In figure 4, the PL spectra of four samples with different sizes are shown by a dotted line, and the absorption spectra are shown by a solid line. We estimated the average radii of the samples other than the ten samples in figure 3, by comparing the energies of their $Z_{1,2}$ exciton absorption band to the energies of the above ten samples. The PL bands are blue-shifted with decrease in the nanocrystal radius. The Stokes shift is clearly seen, as shown by a horizontal bar, and becomes larger with decrease in the radius of the CuBr nanocrystal. The PL band is assigned to free-exciton annihilation, because in the bulk crystal a luminescence band due to the free exciton is found

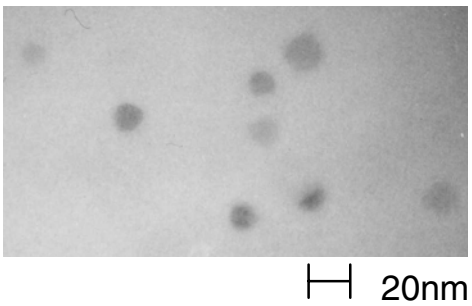

Figure 1. A TEM picture of CuBr nanocrystals with an average radius of 7.0 nm in PMMA.

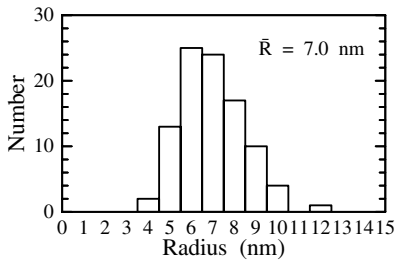

Figure 2. A histogram of the radii of the CuBr nanocrystals shown in figure 1.

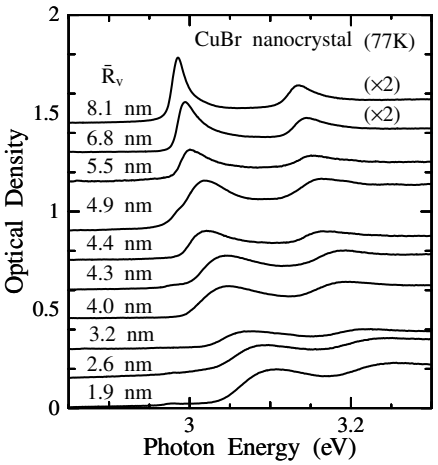

Figure 3. The absorption spectra of PMMA films containing CuBr nanocrystals with different average radii at 77 K.

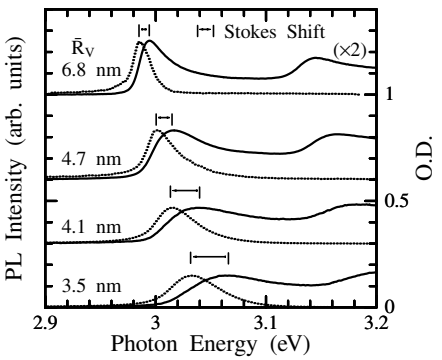

Figure 4. Luminescence (dotted lines) and absorption (solid lines) spectra of CuBr nanocrystals with different average radii in PMMA at 77 K.

very close to the $Z_{1,2}$ absorption band and bound-exciton luminescences disappear at 77 K [3]. The linewidth of the PL band at 77 K is almost the same as the homogeneous linewidth, because it shows no significant narrowing even in resonant excitation at the red edge of the $Z_{1,2}$ absorption band, although this result is not shown here.

On the other hand, the exciton dispersion relation of the bulk crystal has been calculated near the Γ point of the Brillouin zone [10, 11]. We calculate the dispersion relations for a wider range of the wave vector in terms of the $\boldsymbol{k}$-linear theory given by Cho [12] in order to clarify the quantum-size effects on the exciton absorption and PL band energies. According to the $\boldsymbol{k}$-linear theory [12], the energy levels of the Γ_5 and $\Gamma_3 + \Gamma_4$ excitons split into eight levels at a finite wave vector $\boldsymbol{k}$, and the anisotropic dispersion appears. The $\boldsymbol{k}$-linear term in the $\boldsymbol{k}$-dependent mixing is yielded by a spin–orbit interaction at a finite $\boldsymbol{k}$ and an antisymmetric potential. As a consequence of the mixing, the lowest branch of the $Z_{1,2}$ exciton state, which is a dipole-forbidden state at $\boldsymbol{k} = 0$, turns into a dipole-allowed state at a finite $\boldsymbol{k}$. In the nanocrystal, the size-quantized lowest wave vector becomes larger with decreases in size. Hence, it is suggested that the lowest branch of the $Z_{1,2}$ exciton state in CuBr nanocrystals becomes a dipole-allowed state.

First, we consider the Hamiltonian of the $Z_{1,2}$ excitons whose quantization axis is parallel to the $\langle 111 \rangle$ direction. Then, matrix elements of the exciton Hamiltonian can be calculated using the eight bases, i.e. the bases for the $\Gamma_3 + \Gamma_4$ representations with the total angular momentum $J = 2$: $|2, 2\rangle$, $|2, 1\rangle$, $|2, 0\rangle$, $|2, -1\rangle$, $|2, -2\rangle$, and the bases for Γ_5 with $J = 1$: $|1, 1\rangle$, $|1, 0\rangle$, $|1, -1\rangle$. The $|2, 2\rangle$, $|2, 1\rangle$, $|2, 0\rangle$, $|2, -1\rangle$, $|2, -2\rangle$ states are dipole-forbidden spin-triplet states. The $|1, \pm 1\rangle$ states are states of the transverse exciton, and the $|1, 0\rangle$ state is a state of the longitudinal exciton. The exciton Hamiltonian matrix is decomposed into two equivalent 3×3 blocks and two 1×1 blocks, as shown in table 1. The dispersion curves of the $Z_{1,2}$ exciton along the $\langle 111 \rangle$ direction are calculated from the Hamiltonian in table 1, and are shown in figure 5(a). The upper abscissa represents the size-quantized lowest $\boldsymbol{k}$ in the nanocrystal with the radius indicated. The dispersion curves along $\langle 110 \rangle$ and $\langle 100 \rangle$ directions are also shown in figures 5(b) and 5(c), respectively. The parameters used in the calculation are the same as those for the bulk crystal [13], as shown in table 2. Branches 4 and 5, whose numbers are shown on the right-hand side of figure 5(a), are associated with the $|2, 0\rangle$ and $|1, 0\rangle$ states, respectively. Branches 1, 2, and 3 are mixtures of $|2, \pm 2\rangle$, $|2, \pm 1\rangle$, $|1, \pm 1\rangle$ states.

Table 1. The Hamiltonian for $\boldsymbol{k} \parallel \langle 111 \rangle$. $G^2 = \hbar^2 k^2/(2m_0)$, $T = (\sqrt{3}/2\sqrt{2})\hbar K_l^{\mathrm{ex}} k$, m_0 is a free-electron mass, and $\hbar K_l^{\mathrm{ex}}$ is the coefficient of the $\boldsymbol{k}$-linear term for the exciton. γ_1^{ex}, γ_2^{ex}, and γ_3^{ex} are the Luttinger parameters [11, 13]. E_{LT} is the longitudinal–transverse splitting energy owing to the dipole–dipole interaction, and E_{Tt} is the short-range exchange energy [11, 13].

			$\|1, 0\rangle$
			$(E_{\mathrm{LT}} + E_{\mathrm{Tt}} + (\gamma_1^{\mathrm{ex}} + 2\gamma_3^{\mathrm{ex}})G^2)$
			$\|2, 0\rangle$
			$((\gamma_1^{\mathrm{ex}} + 2\gamma_3^{\mathrm{ex}})G^2)$
$\|2, \pm 2\rangle$	$\|2, \pm 1\rangle$	$\|1, \pm 1\rangle$	
$(\gamma_1^{\mathrm{ex}} - 2\gamma_3^{\mathrm{ex}})G^2$	T	$\sqrt{3}T$	
T	$(\gamma_1^{\mathrm{ex}} + \gamma_3^{\mathrm{ex}})G^2$	$-\sqrt{3}\gamma_3^{\mathrm{ex}}G^2$	
$\sqrt{3}T$	$-\sqrt{3}\gamma_3^{\mathrm{ex}}G^2$	$E_{\mathrm{Tt}} + (\gamma_1^{\mathrm{ex}} - \gamma_3^{\mathrm{ex}})G^2$	

We assume that only the transverse branches $|1, \pm 1\rangle$ contribute to photogeneration of the excitons in CuBr nanocrystals, and that the longitudinal branch and spin-triplet branches are not involved. The wave function $|\Phi\rangle$ after taking account of the $\boldsymbol{k}$-linear mixing is

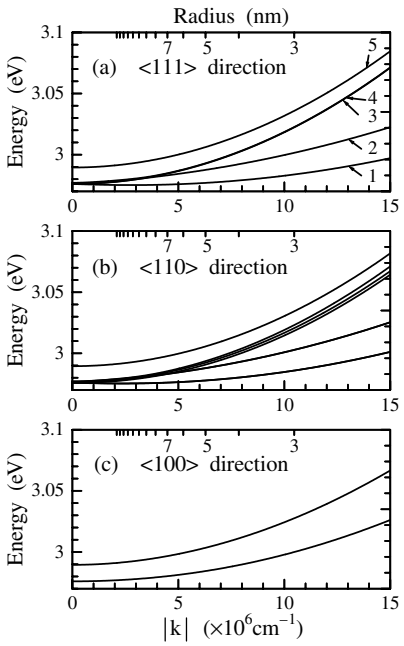

Figure 5. (a) The dispersion curves of five branches associated with the $Z_{1,2}$ exciton along the ⟨111⟩ direction calculated according to Cho's $\boldsymbol{k}$-linear theory. The branch number is indicated at the right-hand edge of each curve. The parameters used in the calculation are the same as those for the bulk crystal. The upper abscissa represents the size-quantized lowest $\boldsymbol{k}$ in the nanocrystal with the radius indicated. (b), (c) The exciton dispersion curves along the ⟨110⟩ and ⟨100⟩ directions, respectively.

Table 2. Values [13] of the parameters in table 1.

γ_1^{ex}	γ_3^{ex}	$\hbar K_l^{ex}$ (10^{-10} eV cm)	E_{LT} (meV)	E_{Tt} (meV)
0.75	0.18	6.9	12.5	1.0

described by

$$|\Phi\rangle = \sum_i a_i|\phi_i\rangle + \sum_j b_j|\psi_j\rangle \tag{3.1}$$

where $|\phi_i\rangle$ is the transverse state and $|\psi_j\rangle$ is the longitudinal or the spin-triplet state. We define the relative oscillator strength (f_{ros}) as

$$(f_{ros}) = \sum_i |a_i|^2 \Big/ \left(\sum_i |a_i|^2 + \sum_j |b_j|^2\right). \tag{3.2}$$

(f_{ros}) along the ⟨111⟩ direction is shown as a function of the wavenumber in figure 6. The numbers in figure 6 correspond to those in figure 5(a). The branches 1, 2, and 3 in figure 5(a) may correspond to the three exciton states of the $Z_{1,2}$ exciton which are considered in the study of the excitation spectra in reference [8], because their values of (f_{ros}) are finite at $k \neq 0$. This means that the states are dipole-allowed states in nanocrystals. (f_{ros}) is assumed to be proportional to the exciton absorption band area in nanocrystals because the energy differences among the exciton branches are too small to be detected separately in the absorption spectrum. Then, the peak energy of the $Z_{1,2}$ exciton absorption band is represented by the mean energy

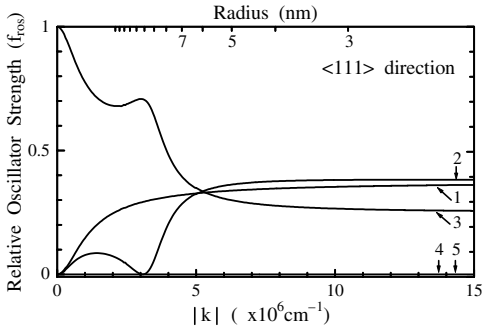

Figure 6. The relative oscillator strengths along the ⟨111⟩ direction for different branches.

A_{mean}, written as

$$A_{\mathrm{mean}} = \sum_l E_l (f_{\mathrm{ros}})_l \tag{3.3}$$

where l denotes an exciton branch, E_l is the energy of branch l, and $(f_{\mathrm{ros}})_l$ is (f_{ros}) for branch l. Generally, an exciton formed in the nanocrystal by an incident photon is relaxed to lower-energy branches and then recombines radiatively in the thermal equilibrium state. Hence, the peak energy of the $Z_{1,2}$ exciton luminescence is represented by the energy P_{eq}:

$$P_{\mathrm{eq}} = \sum_l E_l (f_{\mathrm{ros}})_l \left[\exp(-E_l/k_{\mathrm{B}}T) \Big/ \left(\sum_i \exp(-E_i/k_{\mathrm{B}}T) \right) \right] \tag{3.4}$$

where k_{B} is Boltzmann's constant and T is the temperature.

In the nanocrystal, the lowest quantized $\boldsymbol{k}$ increases with decrease in the radius, while (f_{ros}) for the lowest-energy-state exciton increases as the nanocrystal radius decreases.

In the nanocrystal, the above calculation is carried out for the wave vector $\boldsymbol{k}$ in the ⟨111⟩ direction. In a real nanocrystal, however, the confinement directions are uniformly distributed. Hence, we have to calculate the mean energy over all directions to compare the radius dependence of the $Z_{1,2}$ exciton absorption and PL energies. For simplicity, the mean energy of the $Z_{1,2}$ excitons for all directions is calculated as

$$A_{\mathrm{mean}}^{\langle \text{all directions} \rangle} = \frac{A_{\mathrm{mean}}^{\langle 111 \rangle} \times 8 + A_{\mathrm{mean}}^{\langle 110 \rangle} \times 12 + A_{\mathrm{mean}}^{\langle 100 \rangle} \times 6}{26} \tag{3.5a}$$

$$P_{\mathrm{mean}}^{\langle \text{all directions} \rangle} = \frac{P_{\mathrm{mean}}^{\langle 111 \rangle} \times 8 + P_{\mathrm{mean}}^{\langle 110 \rangle} \times 12 + P_{\mathrm{mean}}^{\langle 100 \rangle} \times 6}{26} \tag{3.5b}$$

where $A_{\mathrm{mean}}^{\langle ijk \rangle}$ ($P_{\mathrm{mean}}^{\langle ijk \rangle}$) is the mean energy A_{mean} (P_{mean}) along the $\langle ijk \rangle$ direction. When 26 axes are drawn from the origin isotropically, there are 8 axes equivalent to the ⟨111⟩ axis, 12 axes equivalent to the ⟨110⟩ axis, and 6 axes equivalent to the ⟨100⟩ axis. Figure 7 shows the experimental peak energies of the $Z_{1,2}$ exciton absorption band (solid circles) and the PL band (open squares) as a function of $\bar{R}_{\mathrm{v}}/a_{\mathrm{B}}$, where a_{B} is the exciton Bohr radius (1.25 nm) in CuBr crystals. The optical density of the samples is so low that the energy shift of the PL peak due to correction of maximum re-absorption effect is only a few meV. Thus, we neglect the re-absorption effects here. The mean energies of the $Z_{1,2}$ exciton absorption ($A_{\mathrm{mean}}^{\langle \text{all directions} \rangle}$) and PL ($P_{\mathrm{mean}}^{\langle \text{all directions} \rangle}$) bands calculated from equations (3.5*a*) and (3.5*b*) are shown by curves A and B in figure 7, respectively. Curves C and D are calculated from curves A and B by taking account of the dead-layer effect. Here, we use the dead-layer thickness of $1.9a_{\mathrm{B}}$ as an

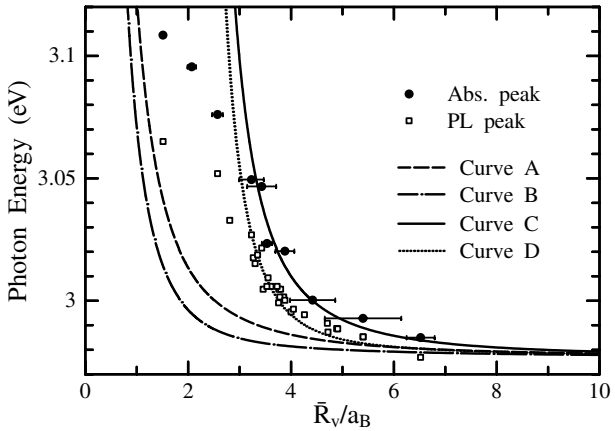

Figure 7. Solid circles and open squares show the experimental peak energies of the absorption and PL bands, respectively, as a function of $\bar{R}_v/a_B$. Curves A and B represent the average absorption and PL dispersions calculated using equations (3.5*a*) and (3.5*b*). Curves C and D represent the average absorption and PL dispersion corrected by taking the dead-layer effect into account, where the thickness of the dead layer is assumed to be $1.9a_B$.

adjustable parameter. Reliability of this value is discussed later. Curves C and D coincide with the experimental blue-shift of the peak energies of the $Z_{1,2}$ exciton absorption band and the PL band in the range $\bar{R}_v/a_B \geqslant 3.5$. On the other hand, the curves C and D deviate from the experimental blue-shifts in the range $\bar{R}_v/a_B < 3.5$. This difference may be caused by the nanocrystal being too small to be analysed using the parameters of the bulk crystal, and the exciton confinement model being no longer correct because of the individual confinements of the electron and hole.

Next, we examine how reasonable of the dead-layer thickness is. In real nanocrystals, the dead layer is composed of two components. One is a surface roughness layer (d_1) into which an electron or a hole cannot enter, and the other is a layer (d_2) in which the centre of mass of an exciton cannot exist. We assumed the thickness of the former layer to be almost the same as the thickness of one atomic layer ($d_1 = 0.46a_B$), and thus $d_2 = (1.9–0.46)a_B = 1.44a_B$. Kayanuma reported quantum-size effects of an electron–hole system confined in semiconductor nanocrystals [14]. In Kayanuma's paper, numerical calculation of the energies of the electron–hole system is carried out using Ritz's variational technique. In the range $R/a_B \geqslant 4$, the numerical values obey formula (1.1) only when the dead layer (d) is chosen as $0.73a_B$, $1.1a_B$, and $1.4a_B$ for $m_h/m_e = 1, 3, 5$, respectively. Here, m_h and m_e are the effective masses of a hole and an electron in a semiconductor crystal. For the CuBr crystal, $m_h/m_e = 5$ [15]. Then, the adjustable parameter $d_2 = 1.44a_B$ is very close to the theoretical value $d = 1.4a_B$, because d is equivalent to d_2 for real nanocrystals.

On the other hand, in a study of CdSe nanocrystals at 10 K or less [16], Nirmal *et al* suggested that the band shape of the exciton PL depends on the strength of the coupling between the exciton and the LO phonon. In the case of CuBr nanocrystals at 77 K, the half-width of the PL band in figure 4 is smaller than the LO-phonon energy (20.7 meV) in the range $\bar{R}_v/a_B \geqslant 3.5$. Hence, the LO-phonon sideband can be distinguished from the zero-phonon band. On the low-energy side of the PL band, however, no shoulder is observed. This means that the PL band mainly consists of the zero-phonon band. It is concluded that the exciton–LO-phonon coupling of CuBr nanocrystals at 77 K is very weak, in contrast to the case for CdSe nanocrystals at 10 K or less.

Therefore, in the range $\bar{R}_v/a_B \geqslant 3.5$, the quantum-size effects of the absorption band and the PL energies due to the $Z_{1,2}$ exciton in CuBr nanocrystals can be interpreted on the basis of a $\boldsymbol{k}$-linear theory.

4. Summary

We have studied quantum-size confinement of exciton energies in CuBr nanocrystals embedded in PMMA. Both the peak energies of the absorption and luminescence bands due to the $Z_{1,2}$ excitons at 77 K are blue-shifted with decreases in the radius of the nanocrystal, and these shifts are associated with a quantum-size effect. The Stokes shift of the PL band becomes larger when the crystal radius decreases. The origin of the Stokes shift is clarified by Cho's $\boldsymbol{k}$-linear theory and size quantization of the exciton wave vector. That is, in CuBr nanocrystals, the mixing among eight branches of the $Z_{1,2}$ exciton depends on the size of the nanocrystal. It is found that the lowest-branch exciton becomes a dipole-allowed state and contributes to the appearance of the PL Stokes shift in CuBr nanocrystals.

Acknowledgments

This work was supported by a Grant-in-Aid for Scientific Research from the Ministry of Education, Science and Culture of Japan. We are grateful to Mr Y Murakami and Mr S Itoh, of the Institute for Materials Research, Tohoku University, Mr F Sato, of the Research Institute for Scientific Measurement, Tohoku University, and Mr T Kawasaki of the Biological Institute, Tohoku University, for taking the TEM pictures of the CuBr nanocrystals.

References

[1] Cardona M 1963 *Phys. Rev.* **129** 69
[2] Sakoda S and Onodera Y 1971 *J. Phys. Chem. Solids* **32** 1365
[3] Goto T, Takahashi T and Ueta M 1968 *J. Phys. Soc. Japan* **24** 314
[4] Ekimov A I and Onushchenko A A 1982 *Sov. Phys.–Semicond.* **16** 775
[5] Ekimov A I, Efros Al L and Onushchenko A A 1985 *Solid State Commun.* **56** 921
[6] Itoh T and Furumiya M 1991 *J. Lumin.* **48+49** 704
[7] Li Y, Takata M and Nakamura A 1998 *Phys. Rev.* B **57** 9193
[8] Itoh T, Iwabuchi Y and Kirihara T 1988 *Phys. Status Solidi* b **146** 531
[9] Yao H and Hayashi T 1992 *Chem. Phys. Lett.* **197** 21
[10] Bivas A, Phach Vu Duy, Hönerlage B, Rössler U and Grun J B 1979 *Phys. Rev.* B **20** 3442
[11] Hönerlage B, Rössler U, Phach Vu Duy, Bivas A and Grun J B 1980 *Phys. Rev.* B **22** 797
[12] Cho K 1976 *Phys. Rev.* B **14** 4463
[13] Nozue Y 1982 *J. Phys. Soc. Japan* **51** 1840
[14] Kayanuma Y 1988 *Phys. Rev.* B **14** 9797
[15] Yu C I, Goto T and Ueta M 1973 *J. Phys. Soc. Japan* **34** 693
[16] Nirmal M, Murray C B and Bawendi M G 1994 *Phys. Rev.* B **50** 2293